2026 IEEE/SICE International Symposium on System Integration (SII)
January 11-14, 2026. Cancún, México

Team Sports Coaching System Using Vibrotactile Feedback

Jose Victorio Salazar Luces, Ankit A. Ravankar, Masahiro Shiratori, Yasuhisa Hirata

***Abstract*— Recent advances in sports coaching technology enable feedback via two main approaches: (a) terminal feedback, which provides performance metrics after gameplay, and (b) continuous feedback, which delivers real-time cues through methods like vibrotactile or auditory stimuli. However, most systems focus on individual performance, making them unsuitable for team sports, where coordinated movements and strategies are essential. This paper proposes a framework for real-time, simultaneous guidance in team sports. The system tracks player positions using a single RGB camera and provides continuous vibrotactile feedback, preserving auditory and visual attention for gameplay. The key contributions are: a lightweight player tracking system using YOLOv4 and coordinate transformations, achieving position estimates at 20 Hz, and a simultaneous vibrotactile guidance system that enables teams to form target formations by following the stimuli. We validate our system through two experiments. First, we assess the tracking accuracy in a virtual environment with four color-tagged moving models, analyzing RMSE across different speeds. Second, we evaluate the effectiveness of vibrotactile guidance by tracking and guiding two subjects through six target formations while measuring performance metrics.**

I. INTRODUCTION

The rise of data analytics has transformed fields such as sports, healthcare, and rehabilitation. Metrics derived from video analysis and wearable devices, including smartwatches and fitness bands, are now widely used in sports instruction. As these technologies become more affordable and accessible, they enable advanced performance analytics while reducing the need for manual coaching. However, most existing technologies focus on individual athletes, limiting their applicability to team sports, where coordinated movement and formations are crucial.

This study proposes a system for real-time tracking and simultaneous guidance of multiple players using vibrotactile feedback. By leveraging a single RGB camera for position estimation, our approach extends the range of our previous methods [1], making it more practical for in-game use. Additionally, vibrotactile stimuli convey intended motion, enabling seamless real-time instruction without disrupting players' auditory or visual focus.

II. RESEARCH BACKGROUND

Existing team sport coaching systems fall into two main categories: (a) post-game/practice performance analysis and (b) real-time information delivery during gameplay.

J. Salazar, A. A. Ravankar, M. Shiratori and Y. Hirata are with the Department of Robotics, Tohoku University, Sendai, Miyagi 980-8579, Japan j.salazar, ankit, m.shiratori, hirata@srd.mech.tohoku.ac.jp

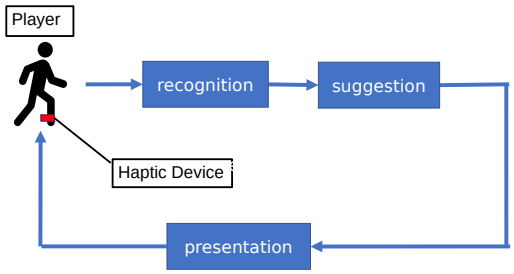

Fig. 1: Block diagram of each process of the proposed system.

In the first category, Suzuki et al. used deep learning to predict tactical patterns in soccer based on player positioning extracted from match videos [2]. Wu et al. developed ForVizor, a formation analysis system that tracks spatio-temporal changes in soccer formations to support expert analysis [3]. These systems enable coaches and analysts to assess player fatigue, movement patterns, and tactical decisions using metrics such as player positions and distances traveled.

In the second category, some systems provide real-time feedback to players. Mostafavi et al. used RFID tags to track player locations, predicting potential collisions and issuing vibration alerts [4]. Sano et al. developed a system combining a ceiling-mounted projector for color-coding opponents and a waist-mounted vibration device to indicate nearby players [5].

Other approaches focus on individual player training. Lamaarti et al. designed a soccer sprinting training system with pressure sensors in shoe insoles and a vibration device for remote coaching via a tablet [6].

A. Human guidance using vibrotactile stimulation

Vibrotactile devices have been widely used for navigation and guidance. Aggravi et al. developed a system for visually impaired skiers using vibration and voice feedback, with vibrating actuators attached to both arms [7]. Amemiya et al. guided users along a grid-like course using a device that leverages the pseudo-attraction force generated by asymmetric vibration [8]. Günther et al. introduced the TactileGlove, which uses multiple vibration actuators to guide the hand to a target in 3D space [9].

Other systems focus on directional navigation. Prasad et al. created the HaptiGo vest, which uses vibrating elements to convey four directional cues [10]. Xu et al. designed a shoe-based device for visually impaired users, providing movement instructions in four directions [11]. Schaach et al.

978-1-6654-5784-2/26/$31.00 ©2026 IEEE

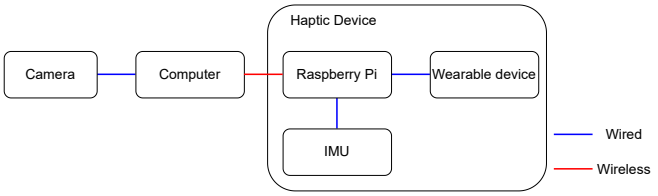

Fig. 2: Hardware configuration of the proposed system.

demonstrated that a neck-worn system with eight actuators can communicate eight directions [12].

For sports applications, Shiraishi et al. developed a belt with 13 vibration actuators, enabling guidance in approximately 12 directions for running athletes [13]. This system was later used to notify players of opponents behind them via vibration stimuli [14].

In the past, our research group proposed a vibrotactile device leveraging the Phantom-Tactile Sensation (PTS) illusion, which can present 360-degree directional cues using only six actuators [15]. When worn on the ankle, this device successfully guided walking users to target locations [16]. In this study, we extend this approach to guide multiple players simultaneously, enabling dynamic formation adjustment, an application not previously explored, to the best of our knowledge.

III. Team Sport Coaching System Using Vibrotactile Feedback

A. System Concept

The proposed system is designed for team sports such as basketball and futsal, where coordinated team movements are crucial. A camera positioned to cover the entire field tracks players, who wear a vibrotactile device on their right ankle to receive directional movement cues.

Our system builds upon Ozaki et al.'s four-step coaching framework for ice skating [17], which includes observation, analysis, decision-making, and instruction. We adapt this into a three-step process for team sports:

- Recognition: Tracking player positions using an RGB camera and IMU sensors.
- Suggestion: Determining an optimal formation based on field conditions.
- Presentation: Delivering vibrotactile cues to guide players toward their target positions.

The block diagram of the proposed system is shown in Fig. 1.

B. Hardware Configuration

The system (Fig. 2) consists of a web camera for full-field image capture, a PC for processing sensor data and controlling feedback, a wearable vibrotactile units powered by Raspberry Pi 3 Model B+ and an IMU to detect each player's body orientation.

By integrating these components, the system provides real-time, intuitive guidance to multiple players, enhancing team coordination without visual or auditory distractions.

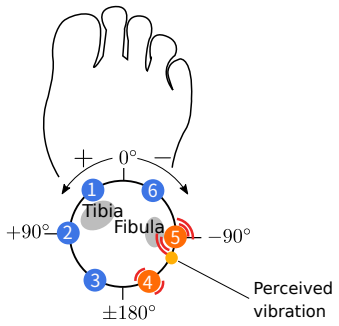

Fig. 3: Arrangement of vibration motors.

TABLE I: Correspondence of the position of PTS cue and actuated motors.

Position of PTS Cue	Actuated Motors
-180° to -150°	Motor 3 and Motor 4
-150° to -90°	Motor 4 and Motor 5
-90° to -30°	Motor 5 and Motor 6
-30° to 30°	Motor 6 and Motor 1
30° to 90°	Motor 1 and Motor 2
90° to 150°	Motor 2 and Motor 3
150° to 180°	Motor 3 and Motor 4

C. Direction guidance by using Vibration Stimuli

The system uses a vibrotactile device on the right ankle to indicate movement direction via the Phantom Tactile Sensation (PTS) illusion [18]. This illusion creates a virtual vibration between two actuators, with its position controlled by varying vibration intensity ratios [19]. We apply the Energy Model by Israr et al. [20], [21] to calculate the intensity of the actuators , and use our previous approach [15], [22] to create these precise directional cues.

D. Vibration Device Setup

Six vibration actuators (HAPTIC™Reactor LRA, Alps Alpine) are evenly spaced around the ankle (Fig.3), covering a range from -180° to +180°. The mapping between PTS cues and actuated motors is detailed in TableI.

In addition, it is necessary to let the subject know in advance how to respond to the produced vibrotactile cue. The two most common conceptual mappings are called "Pull" and "Push". The "Pull" mapping should be interpreted as being pulled by the vibration stimulus, so the user is instructed to move in the same direction where the stimulus was produced. The "Push" mapping represents being pushed away by the vibration stimulus, so users are instructed to move away from the vibration. Users follow a "Pull" mapping, moving toward the perceived vibration, as prior studies showed it leads to faster response times and greater accuracy [15].

The wearable device (Fig. 4) consists of:

- Six actuators, attached via adjustable 3D-printed modules and an elastic band.
- An IMU, filtered using the Madgwick filter [23] for torso orientation tracking.
- A controller unit, using a PCA9685 servo driver and Darlington Array for PWM control.

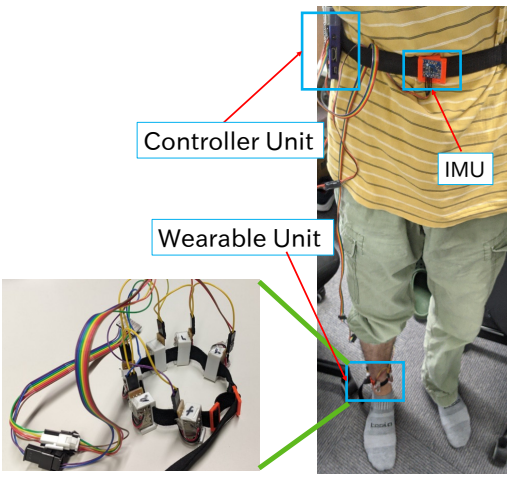

Fig. 4: Vibrotactile feedback device.

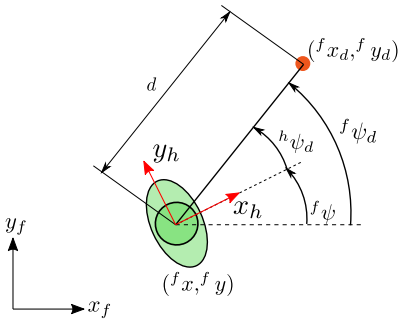

Fig. 5: Person's position and heading angle.

Vibration motors operate at 180 Hz, optimizing sensitivity for Pacinian corpuscles while staying near the actuator's resonance frequency (160 Hz – 200 Hz).

E. Direction Calibration and Guidance

To ensure correct directional guidance, the target direction in the global frame must align with the user's local frame. Given a user's position $({}^f x, {}^f y)$ and orientation ${}^f\psi$, along with the target position $({}^f x_d, {}^f y_d)$, the global target angle is computed as:

$$ {}^f\psi_d = \arctan \frac{{}^f y_d - {}^f y}{{}^f x_d - {}^f x} \tag{1} $$

The relative target direction in the user's local frame is then:

$$ {}^h\psi_d = {}^f\psi_d - {}^f\psi \tag{2} $$

By generating vibrations at ${}^h\psi_d$, the system ensures consistent directional cues regardless of user orientation (Fig. 5).

F. Player Tracking System using Color Tags

The proposed player tracking system is depicted in Fig. 6. It estimates the real-time field coordinates of each player,

Fig. 6: Structure of the proposed image processing system.

Fig. 7: Example of input Bounding Boxes and predicted Bounding Boxes(white square:input bounding box, green square:predicted bounding box).

${}^f\boldsymbol{p}_h = ({}^f x_h, {}^f y_h)$, using a single RGB camera that captures the entire field. To identify players, the system employs person detection alongside color-coded vests and bandanas, enabling real-time recognition without requiring high-resolution or multiple cameras.

Player detection is performed using YOLOv4 [24], a fast object detector that classifies objects and generates bounding boxes indicating their locations. Bounding boxes labeled as "person" are selected, and their screen coordinates, ${}^s\boldsymbol{p}_h = ({}^s u_h, {}^s v_h)$, are transformed into field coordinates, ${}^f\boldsymbol{p}_h = ({}^f x_h, {}^f y_h)$, using the following equation:

$$ \begin{bmatrix} {}^f x_h \\ {}^f y_h \\ {}^f z_h \end{bmatrix} = {}^f_c\boldsymbol{R} \left(\boldsymbol{K}^{-1} s \begin{bmatrix} {}^s u_h \\ {}^s v_h \\ 1 \end{bmatrix} - {}^c_f\boldsymbol{t} \right) \tag{3} $$

where ${}^f_c\boldsymbol{R}$ and ${}^c_f\boldsymbol{t}$ represent the rotation matrix from the field coordinate system to the camera coordinate system and the translation vector from the camera coordinate system to the field coordinate system, respectively, also called the camera's extrinsic parameters, obtained using the solvePnP function in OpenCV [25], $\boldsymbol{K}^{-1}$ is the inverse of the intrinsic camera matrix, s is a scale factor corresponding to the depth of the player along the camera's optical axis and ${}^f z_h$ represents the player's position along the vertical axis of the field coordinate system. Since the system assumes players are mostly upright, ${}^f z_h$ is estimated using a predefined standing height. This assumption simplifies the coordinate transformation process while maintaining accuracy for player tracking.

G. Bounding Box Validation

To filter false detections, the system analyzes the bounding box shape. Three error cases are considered:

- Partial occlusion due to another player.
- Incorrect classification of non-human objects.

Algorithm 1 False positive confirmation algorithm

procedure DETECTFP(inputBB[])
▷ fieldTh: the extent of the field and pre-defined ▷ isTP[i]: indicates if inputBB[i] is true positive or not
  for $i = 0 \ldots$ inputBB[].length $- 1$ **do**
    predBB[i] = predictBB(inputBB[i])
    thWidth=calcThWidth(inputBB[i])
    thHeight=calcThHeight(inputBB[i])
    if inputBB[i].width not in thWidth **then**
      isTP[i]=false
    else
      hRate=inputBB[i].height/predBB[i].height
      if hRate in thHeight **then**
        x,y = transformToField(inputBB[i])
      else
        isOccluded=ISOCL(predBB[i],inputBB[])
        if isOccluded **then**
          x,y=transformToField(predBB[i])
        else
          isTP[i]=false
        end if
      end if
      if x, y in fieldTh **then**
        isTP[i]=true
      else
        isTP[i]=false
      end if
    end if
  end for
end procedure

Algorithm 2 Occlusion confirmation algorithm

procedure ISOCL(predBB[i],inputBB[]) ▷ Initialize the variable s for the sum of the IoU
  $s = 0$
  for $j = 0 \ldots$ inputBB[].length $- 1$ **do**
    if $j \neq i$ **then**
      $s =$ calcIoU(predBB[i], inputBB[j]) $+s$
    end if
  end for
  if $s > 0$ **then**
    return true
  else
    return false
  end if
end procedure

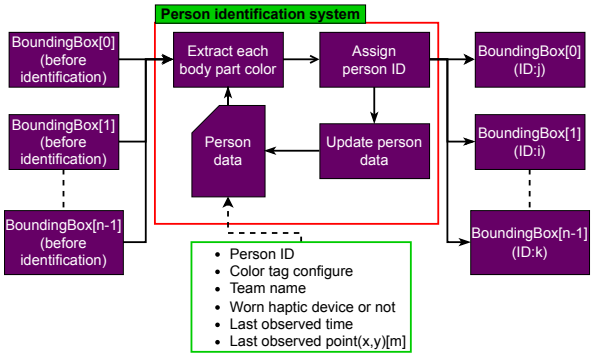

Fig. 8: Structure of the proposed person identification system.

- Misidentification of body parts or multiple players as a single bounding box.

To address the first issue, the system models the human body as a 1.75[m] tall, 0.4[m] diameter cylinder and generates a predicted bounding box. Fig. 7 illustrates a comparison between input and predicted bounding boxes, where significant differences indicate occlusion. The other two error cases are considered false positives. This process is depicted in Algorithm 1.

Algorithm 2 evaluates the bounding box anomaly cause. If occlusion is detected, the system replaces the input bounding box with the predicted one. Occlusion detection relies on the Intersection over Union (IoU) metric:

$$\text{IoU} = \frac{\text{Area of Intersection}}{\text{Area of Union}} \tag{4}$$

H. Player Identification via Color Tags

After detecting players, their identities are determined using color tags. Fig. 8 shows the system structure. Each bounding box is assigned a personal ID by extracting color components and matching them to pre-registered player data.

Identification is achieved using two feature values:

- Spatial consistency: Evaluates position continuity based on previous detections.
- Appearance features: Extracted from color tags.

A weighted linear sum of these features forms a feature matrix, which is processed using the Hungarian algorithm to maximize assignment accuracy.

IV. EXPERIMENTS AND DISCUSSION

A. Player Tracking Accuracy in a Virtual Space

Accurately obtaining the ground truth positions of moving players in a wide area is challenging. Therefore, we first evaluated the accuracy of the player tracking system in a virtual environment. We used the 3D physics simulator Gazebo to create a controlled test scenario, where four humanoid models wearing color tags moved within a predefined area. Each model followed the same route for 60 seconds under eight different velocity conditions.

A virtual camera (1280 $\times$ 720, 60 fps) was positioned to capture the entire field, providing input images for the image processing system. The camera's position and orientation were determined using four corner points of the field, consistent with the real-world setup. Fig. 9 shows a sample image of the virtual environment captured by the camera.

To evaluate tracking accuracy, we varied the average movement speed of the four models and compared the Root Mean Square Error (RMSE) of their tracked positions under

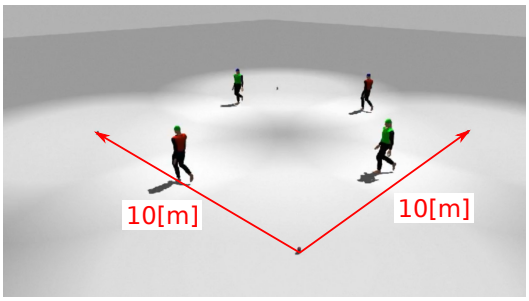

Fig. 9: Image of this experiment from a fixed camera in the Gazebo world

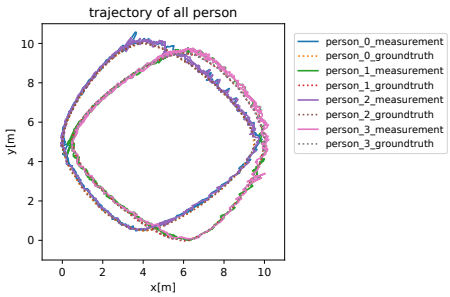

Fig. 10: Trajectories of all persons in a virtual space(mean moving speed:0.72[m/s]).

each speed condition. The RMSE is computed as:

$$\mathrm{RMSE}[m] = \sqrt{\frac{1}{N}\sum_{i=0}^{N}({}^{f}\boldsymbol{p}_{\mathrm{m}i} - {}^{f}\boldsymbol{p}_{\mathrm{gt}i})^{t}({}^{f}\boldsymbol{p}_{\mathrm{m}i} - {}^{f}\boldsymbol{p}_{\mathrm{gt}i})} \quad (5)$$

where N represents the number of tracked positions obtained by the image processing system for a given experimental condition, ${}^{f}\boldsymbol{p}_{\mathrm{m}i}$ denotes the position estimated by the image processing system at time i, and ${}^{f}\boldsymbol{p}_{\mathrm{gt}i}$ denotes the ground truth position obtained directly from the simulation.

The ground truth data was recorded at approximately 100 [Hz], while the image processing system operated at around 20 [Hz]. Due to this difference in sampling rates, position pairs were considered temporally aligned if their timestamps differed by less than 10 [ms].

The measured and true values for the mean moving speeds of 0.72 [m/s] and 5.67 [m/s] are shown in Fig.11.

The results can be seen in Fig. 10 and Fig.11. Fig. 10 compares the ground truth and tracked trajectories for a model moving at an average speed of 0.72 [m/s]. Fig. 11 presents the position difference in x and y for models moving at speeds of 5.67 [m/s].

As shown in Fig. 12, the RMSE increases as the average moving speed increases. The minimum observed error is approximately 0.2 m, while the maximum reaches about 1.0 m. Two factors likely contribute to this trend: (a) processing delay: The object detector YOLOv4 operates at approximately 20 FPS. As the model moves faster, the delay in detecting and processing its position increases, leading

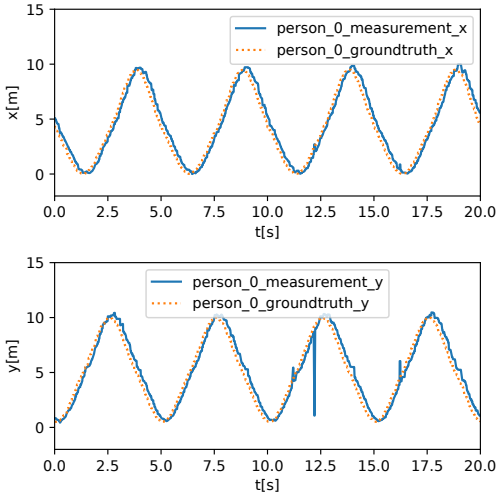

Fig. 11: Trajectories of person 0 vs time in a virtual space(mean moving speed:5.67[m/s]).

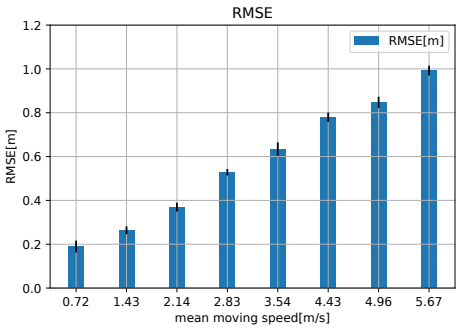

Fig. 12: Average RMSE in each velocity condition.

to greater tracking error, (b) increased occlusion: Since all models follow the same path for 60 seconds under each speed condition, the frequency of occlusions increases at higher speeds. This results in more tracking errors, as overlapping bounding boxes interfere with accurate player localization. These findings suggest that while the system performs well at lower speeds, future improvements should focus on mitigating occlusion effects and reducing processing delays to enhance tracking accuracy at higher speeds.

B. Formation Guidance Experiment

In this experiment, we verified whether the proposed player tracking system together with the vibration device could be used for simultaneously tracking and guiding multiple users to reach a specific formation or configuration. In other words, we will verify *recognition* and *presentation* of the formation guidance system shown in Fig.1. The experiment was conducted in a 10[m]×10[m] area at the Tohoku University Aobayama Gymnasium under the following conditions. 1) The experiment was conducted by 10 healthy males(aged 22-35), working in teams of 2. 2) Everyone wore

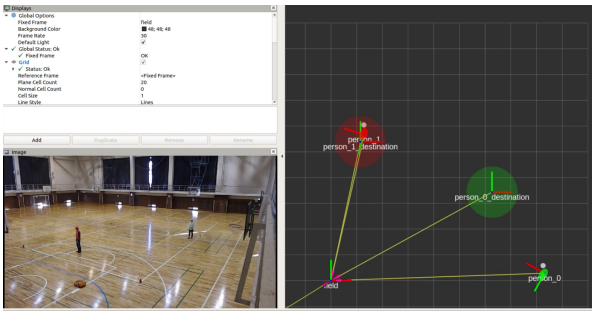

Fig. 13: User interface of a haptic navigation.

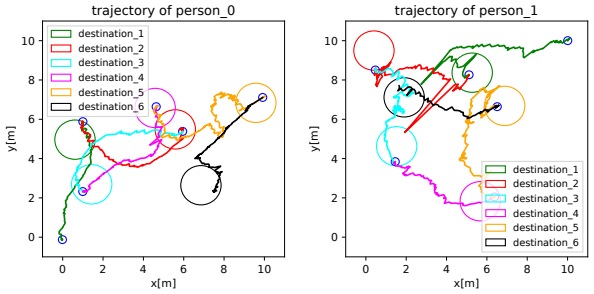

(a) person_0 (b) person_1

Fig. 14: Trajectories and destinations of pair B.

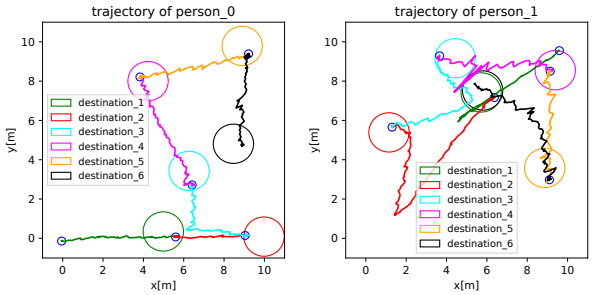

(a) person_0 (b) person_1

Fig. 15: Trajectories and destinations of pair D.

a vibration device on their right ankle and different colored vests and bandanas. 3) A random formation consisting of two points 5[m] away from each other is generated, and feedback is produced to guide them towards their respective position. 4) A subject is judged to have reached the target point if he or she stays within a circle of radius 1[m] centered on the target point for 2 seconds. When they reach a target point, the next point is presented. 5) Subjects practiced for about 3 minutes before performing the experiment in order to familiarize with the device. The position and posture of each subject are acquired from the fixed web camera image and the IMU attached to each subject. This experiment was approved by the Ethics Committee on Research Involving Human Subjects of the Graduate School of Engineering, Tohoku University.

During the experiment, the supervisor checks whether the position and posture of each subject are correctly measured from the user interface displayed on the PC screen as shown in Fig.13. The lower left corner of Fig.13 displays the web camera image, which is the same as the input image of the image processing system. In the center of the screen, the position and posture of each subject in the field coordinates and the position of the target area of each subject are displayed. The color of the target area is the same as that of the subject, and the radius of the circle of the target area displayed on the screen is a circle of radius 1[m], the same as that of the target area in the experiment.

The performances of the system were evaluated using Motion Efficiency ME, Reaching Velocity RV[m/s] and Reaching Time RT[s]. $ME \in [0, 1]$ is an indicator of the straightness of the subject's movement trajectory from the starting point to the destination [26], and evaluates how linearly the subject was able to move in the presented direction. ME is calculated as

$$ME = \frac{E_P}{U_P} \tag{6}$$

where E_P is the straight-line distance from the start point to the target area, which is 1[m] minus the distance between the start point and the center of the target area, since the target area in this experiment is a circle of radius 1[m] centered on the target point. The U_P represents the path length followed by the subject to reach the target position and is calculated by calculating the L2 norm for the continuous data of the subject's position coordinates ${}^f\boldsymbol{p}_i = ({}^f x_i, {}^f y_i)$ measured during the movement and summing them up, as follows

$$U_P = \sum_{i=0}^{N} \sqrt{({}^f\boldsymbol{p}_{i+1} - {}^f\boldsymbol{p}_i)({}^f\boldsymbol{p}_{i+1} - {}^f\boldsymbol{p}_i)^t} \tag{7}$$

Therefore, the unit of ME is a dimensionless quantity, and a ME of 1.0 indicates that the object has traveled the shortest distance, and a ME of 0.5 indicates that the object has traveled twice the shortest distance.

$RV \in [0, 1]$ is a measure of how fast the user reaches the target area from the starting point [26], and is defined by

$$RV[\mathrm{m/s}] = \frac{E_P}{T_P} \tag{8}$$

Here, T_P is the number of seconds taken by the subject to move from the starting point to the target area and obtain an arrival judgment, minus two seconds. In other words, the time spent in the target area until the arrival judgment is obtained is not included in T_P.

As an example of the experimental results, Fig.14 and 15 show the destinations of each subject in pairs B and D and the trajectories of their movements to each destination. Here, the small blue circles represent the starting point for each target region, and the large colored circles and lines represent the target region and the trajectory to the target region.

Here, as shown in Fig.14b, the trajectory from the start point of person_1 to destination 1 (green line) and the

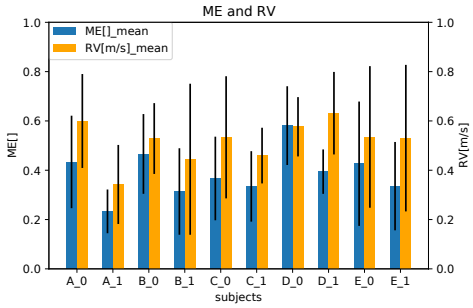

(a) ME and RV for each subject.

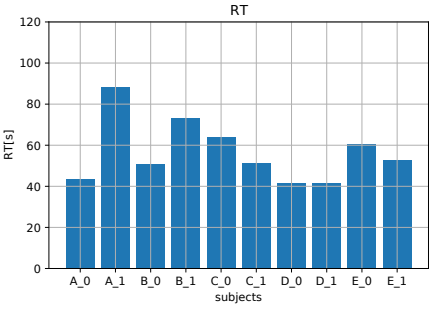

(b) RT for each subject.

Fig. 16: Evaluation indexes of random formation haptic navigation in Aobayama gymnasium.

trajectory from the target area 1 to destination 2 (red line in the figure) changed significantly in the lower left direction. This is due to the occlusion with person_0 and is not the actual movement trajectory. In most cases, the subject rotated on the spot until the vibration stimulus came to the front of the subject's ankle, and when the stimulus came to the front direction, the subject went straight.

The results of each evaluation index are shown in Fig.16a and 16b. Here, the horizontal axis of each graph represents the subject, the alphabet represents the pair of two persons, and the numbers represent person_0 and person_1. The largest mean value of ME was 0.581 for subject D_0, and the largest mean value of RV was 0.631 for subject D_1.

V. DISCUSSION

The results from the experiments seem to indicate that the proposed system is able to track players' positions in the field and guide them to different formations using vibrotactile stimuli.

We think that there are several factors to consider when applying this system to different team sports. For example, while using the ankle might be good for sports like voleyball, where the hands and arms need to be free to interact with the ball, it might be better to use it on the wrist or torso for sports like soccer, where the device could be a nuisance when kicking the ball.

Additionally, even though the player tracking system covers a large area using a single camera, we want to explore using multiple cameras and fusing the information in order to further avoid problems caused by occlusion and false positives. Some subjects commented that the vibration stimuli were not continuous but intermittent, which confused them, even though they were stationary near the target area. This is thought to be caused the accuracy of the player tracking system, and would be solved by improving its accuracy.

VI. CONCLUSIONS AND FUTURE WORK

In this paper, we proposed a concept of a sports coaching system using vibrotactile stimuli, which consists of three components: "recognition", "suggestion", and "presentation". In order to locate players in the field, we developed a player tracking system using a single RGB camera, and succeeded in recognizing four players wearing different color tags within a range of 10[m]×10[m]. The effectiveness of the proposed system in "recognition" and "presentation" was confirmed by guiding users wearing vibration devices to arbitrary formations consisting on two random points 5[m] away from each other. In the future, we will improve the performance of the player tracking system and evaluate the suitability of different vibration presentation methods for actual team sports instruction.

ACKNOWLEDGMENT

This work was partially supported by Japan Science and Technology Agency (JST) [Moonshot R&D Program] under Grant JPMJMS2034. This work was partially supported by JSPS KAKENHI Grant Number 20K19838.

REFERENCES

[1] J. V. S. Luces, K. Ishida, and Y. Hirata, "Human position guidance using vibrotactile feedback stimulation based on phantom-sensation," in *2019 IEEE International Conference on Cyborg and Bionic Systems (CBS)*, 2019, pp. 235–240.

[2] G. Suzuki, S. Takahashi, T. Ogawa, and M. Haseyama, "Team Tactics Estimation in Soccer Videos Based on a Deep Extreme Learning Machine and Characteristics of the Tactics," *IEEE Access*, vol. 7, pp. 153 238–153 248, 2019.

[3] Z. Wu and W. Wang, "Adaptive Anti-Disturbance Method for Magnetometer and INS Integration in a Road Vehicle," *Journal of Navigation*, vol. 72, no. 6, pp. 1513–1532, 2019.

[4] M. Mostafavi, F. Nikseresht, J. E. Resch, L. Barnes, and M. Boukhechba, "Collision Prediction and Prevention in Contact Sports Using RFID Tags and Haptic Feedback," *Lecture Notes in Networks and Systems*, vol. 275, pp. 400–406, 2021.

[5] Y. Sano, K. Sato, R. Shiraishi, and M. Otsuki, "Influence of Visual and Haptic Stimuli on Play Skill in a Ball Game," *Transactions of the Virtual Reality Society of Japan*, vol. 22, no. 4, pp. 493–502, 2017.

[6] F. Lamaarti, F. Arafsha, B. Hafidh, and A. El Saddik, "Automated Athlete Haptic Training System for Soccer Sprinting," *Proceedings - 2nd International Conference on Multimedia Information Processing and Retrieval, MIPR 2019*, pp. 303–309, 2019.

[7] M. Aggravi, G. Salvietti, and D. Prattichizzo, "Haptic assistive bracelets for blind skier guidance," *ACM International Conference Proceeding Series*, vol. 25-27-Febr, 2016.

[8] T. Amemiya and H. Sugiyama, "Haptic handheld wayfinder with pseudo-attraction force for pedestrians with visual impairments," *ASSETS'09 - Proceedings of the 11th International ACM SIGACCESS Conference on Computers and Accessibility*, pp. 107–114, 2009.

[9] S. Günther, J. Kirchner, F. Müller, N. Dezfuli, M. Funk, and M. Mühlhäuser, "TactileGlove: Assistive spatial guidance in 3D space through vibrotactile navigation," *ACM International Conference Proceeding Series*, pp. 273–280, 2018.

[10] M. Prasad, P. Taele, A. Olubeko, and T. Hammond, "Haptigo: A navigational 'tap on the shoulder'," in *2014 IEEE Haptics Symposium (HAPTICS)*. IEEE, 2014, pp. 339–345.

[11] Q. Xu, T. Gan, S. C. Chia, L. Li, J.-H. Lim, and P. K. Kyaw, "Design and evaluation of vibrating footwear for navigation assistance to visually impaired people," in *2016 IEEE International Conference on Internet of Things (iThings) and IEEE Green Computing and Communications (GreenCom) and IEEE Cyber, Physical and Social Computing (CPSCom) and IEEE Smart Data (SmartData)*. IEEE, 2016, pp. 305–310.

[12] S. Schaack, G. Chernyshov, K. Ragozin, B. Tag, R. Peiris, and K. Kunze, "Haptic collar: Vibrotactile feedback around the neck for guidance applications," in *Proceedings of the 10th Augmented Human International Conference 2019*, 2019, pp. 1–4.

[13] R. Shiraishi, K. Sato, Y. Sano, and M. Otsuki, "Haptic directional instruction system for sports," *Lecture Notes in Electrical Engineering*, vol. 432, pp. 361–368, 2018.

[14] Y. Sano, K. Sato, R. Shiraishi, and M. Otsuki, "Player perception augmentation for beginners using visual and haptic feedback in ball game," *26th IEEE Conference on Virtual Reality and 3D User Interfaces, VR 2019 - Proceedings*, pp. 1142–1143, 2019.

[15] J. V. S. Luces, K. Okabe, Y. Murao, and Y. Hirata, "A phantom-sensation based paradigm for continuous vibrotactile wrist guidance in two-dimensional space," *IEEE Robotics and Automation Letters*, vol. 3, no. 1, pp. 163–170, 2017.

[16] Z. Liao, J. V. S. Luces, and Y. Hirata, "Human navigation using phantom tactile sensation based vibrotactile feedback," *IEEE Robotics and Automation Letters*, vol. 5, no. 4, pp. 5732–5739, 2020.

[17] A. Ozaki and M. Honda, "Development of an Automated Motion Coaching System Using a Portable Sensor," *Transactions of Japanese Society for Information and Systems in Education*, vol. 33, no. 1, pp. 22–30, 2016.

[18] G. V. Bekesy, "Sensory inhibition," *Princeton Univ. Press*, vol. 158, no. 3806, pp. 1296–1298, 1967.

[19] D. Alles, "Information Transmission by Phantom Sensations," *IEEE Transactions on Man-Machine Systems*, vol. 11, no. 1, 1970.

[20] A. Israr, H. Z. Tan, J. A. Mynderse, and G. T. Chiu, "A psychophysical model of motorcycle handlebar vibrations," in *In Proceedings of the ASME 2007 International Mechanical Engineering Congress and Exposition*, vol. 9: Mechanical Systems and Control, Parts A, B, and C, 2007, pp. 1233–1239.

[21] A. Israr and I. Poupyrev, "Tactile brush: drawing on skin with a tactile grid display," in *Proceedings of the SIGCHI Conference on Human Factors in Computing Systems*. ACM, 2011, pp. 2019–2028.

[22] J. V. S. Luces, K. Ishida, and Y. Hirata, "Human position guidance using vibrotactile feedback stimulation based on phantom-sensation," *2019 IEEE International Conference on Cyborg and Bionic Systems (CBS)*, pp. 142–147, 2019.

[23] S. O. Madgwick, "An efficient orientation filter for inertial and inertial/magnetic sensor arrays," *Journal of Dental Research*, 2010.

[24] A. Bochkovskiy, C.-Y. Wang, and H.-Y. M. Liao, "YOLOv4: Optimal Speed and Accuracy of Object Detection," 2020. [Online]. Available: http://arxiv.org/abs/2004.10934

[25] V. Lepetit, F. Moreno-Noguer, and P. Fua, "EPnP: An accurate O(n) solution to the PnP problem," *International Journal of Computer Vision*, vol. 81, no. 2, pp. 155–166, 2009.

[26] A. J. Spiers and A. M. Dollar, "Design and evaluation of shape-changing haptic interfaces for pedestrian navigation assistance," *IEEE Transactions on Haptics*, vol. 10, no. 1, pp. 17–28, Jan 2017.